DETERMINATION OF ELECTRON FLUX SPECTRA IN A SOLAR FLARE WITH AN AUGMENTED REGULARIZATION METHOD: APPLICATION TO RHESSI DATA

Eduard P. Kontar*
Department of Physics & Astronomy, University of Glasgow, G12 8QQ, UK

A. Gordon Emslie
Department of Physics, The University of Alabama in Huntsville, Huntsville, AL 35899, USA

Michele Piana
Dipartimento di Matematica, Università di Genova, via Dodecaneso 35, I-16146 Genova, Italy

Anna Maria Massone
INFM, UdR di Genova, via Dodecaneso 33, I-16146 Genova, Italy

John C. Brown
Department of Physics & Astronomy, University of Glasgow, G12 8QQ, UK

Abstract. Kontar et al. (2004) have shown how to recover mean source electron spectra $\overline{F}(E)$ in solar flares through a physical constraint regularization analysis of the bremsstrahlung photon spectra $I(\epsilon)$ that they produce. They emphasize the use of non-square inversion techniques, and preconditioning combined with physical properties of the spectra to achieve the most meaningful solution to the problem. Higher-order regularization techniques may be used to generate $\overline{F}(E)$ forms with certain desirable properties (e.g., higher order derivatives). They further note that such analyses may be used to infer properties of the electron energy spectra at energies well above the maximum photon energy observed. In this paper we apply these techniques to data from a solar flare observed by *RHESSI* on 26 February, 2002. Results using different orders of regularization are presented and compared for various time intervals. Clear evidence is presented for a change in the value of the high-energy cutoff in the mean source electron spectrum with time. We also show how the construction of the *injected* electron spectrum $F_0(E_0)$ (assuming that Coulomb collisions in a cold target dominate the electron energetics) is facilitated by the use of higher-order regularization methods.

Keywords: Sun: flares, Sun: X-rays, Sun: electron spectrum

1. Introduction

The hard X-ray spectrum $I(\epsilon)$ (photons cm^{-2} s^{-1} keV^{-1}) in solar flares is related to the mean electron flux spectrum $\overline{F}(E)$ (electrons cm^{-2} s^{-1} keV^{-1})

* Off-print requests: eduard@astro.gla.ac.uk

through the bremsstrahlung cross-section $Q(\epsilon, E)$ in the defining equation (Brown, Emslie, & Kontar 2003) for $\overline{F}(E)$, viz.

$$I(\epsilon) = \frac{1}{4\pi R^2}\,\overline{n}V \int_{\epsilon}^{\infty} \overline{F}(E)\, Q(\epsilon, E)\, dE, \tag{1}$$

where $Q(\epsilon, E)$ is the isotropic bremsstrahlung cross-section differential in photon energy (cm^2 keV^{-1}), R (cm) is the distance to the observer and the mean target density $\overline{n} = V^{-1} \int n(\mathbf{r})\, dV$ (cm^{-3}). Piana et al. (2003) have shown how zero order regularized solution of Equation (1) for $\overline{F}(E)$ may be obtained through discretization of the equation and addition of a penalty term for recovered solutions that exhibit excessive noise in the solution (cf. Johns & Lin (1992), who address this issue through flexible binning of the photon data). Piana et al. (2003) applied this algorithm to the intense hard X-ray flare of July 23, 2002 (Lin et al., 2003) and derived interesting features in the recovered $\overline{F}(E)$ spectrum (such as a spectrum significantly above the forward-fit [Holman et al. 2003], Maxwellian in the range 20-40 keV, and an apparent dip in the electron spectrum around 55 keV). This analysis, however, used a "square" algorithm, utilizing photon data over the range $10 < \epsilon < 160$ keV to derive the electron spectrum in the same energy range; because of the flatness of the spectrum in this event, they were forced to utilize an extrapolation of the electron spectrum above 160 keV by a power-law tail to adequately account for the (significant) contribution of electrons at energies $E > 160$ keV to the photon emission in the $[10, 160]$ keV range.

As pointed out in the companion paper (Kontar et al. 2004; hereafter Paper I), the hard X-ray spectrum over a finite range $[\epsilon_{\min}, \epsilon_{\max}]$ of photon energies nevertheless contains considerable information on the *electron* spectrum over a much wider range through the relation (1). For example, if $\overline{F}(E)$ has an upper energy cutoff at $E = E_{\max} > \epsilon_{\max}$, then one should still find evidence of this upper energy cutoff in the observed photon spectrum below $\epsilon_{\max}$, because of the requirement that the spectrum tends to zero at $\epsilon = E_{\max}$. As shown in Paper I, use of a generalized (rectangular) regularization method permits a *quantitative* analysis of this high-energy part of the electron spectrum. In this paper, we therefore apply the analysis technique of Paper I to observations of high-resolution hard X-ray spectra obtained with the *Ramaty High Energy Solar Spectroscopic Imager* (RHESSI) (Lin et al., 2002). We show (§2) evidence for just such upper energy cutoffs in the electron spectra in the 26 February, 2002 (about 10:26 UT) solar flare and we discuss the variation of this cutoff energy with time in §3. In §4 we continue the analysis by presenting the *injected* electron flux spectrum $F_0(E_0)$, under the assumption that the mean source electron spectrum

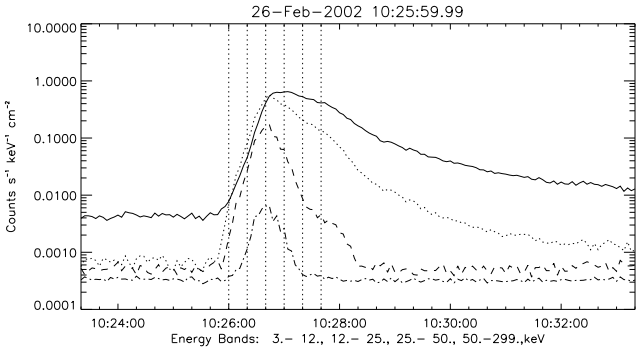

Figure 1. Light curves for the 26 February, 2002 event. The five observational time intervals used in the analysis are shown by vertical dashed lines.

$\overline{F}(E)$ results from the modification of this spectrum in a cold collisional target, and we emphasize the usefulness of higher-order regularization techniques in constructing this injected spectrum. In §5 we present our conclusions.

2. Application to RHESSI Data

We selected the GOES M-class hard X-ray event of 26 February, 2002 (start time $\sim$ 10:26 UT) for our analysis. This event provides sufficiently high count rate for a detailed analysis over wide energy range but does not introduce pulse pile-up issues (Smith et al, 2002). Figure 1 shows the light curves for the photon energy bands $([3-12],[12-25],[25-50],[50-300])$ keV; five time intervals covering the entire impulsive phase of the flare are indicated.

RHESSI (Lin et al., 2002) has nine detectors, each designed to have a 1keV resolution in photon energy. In practice however, detectors 2 and 7 have a poorer resolution than intended (Smith et al., 2002) and so all results presented here are based only on the seven fully functional front segments. We used 1 keV energy bins and time bins equal to RHESSI's rotation period (as given for the time of the flare). This ensured that background and analysis intervals were multiples of the rotation period eliminating any modulation from the imaging grids.

The top left panel of Figure 2 shows the photon spectrum for the second time interval (10:26:20 - 10:26:40 UT), up to a maximum photon energy $\sim$ 160 keV for this time intervals. In the spectrum at energies higher than 160 keV, the uncertainties are comparable to the signal

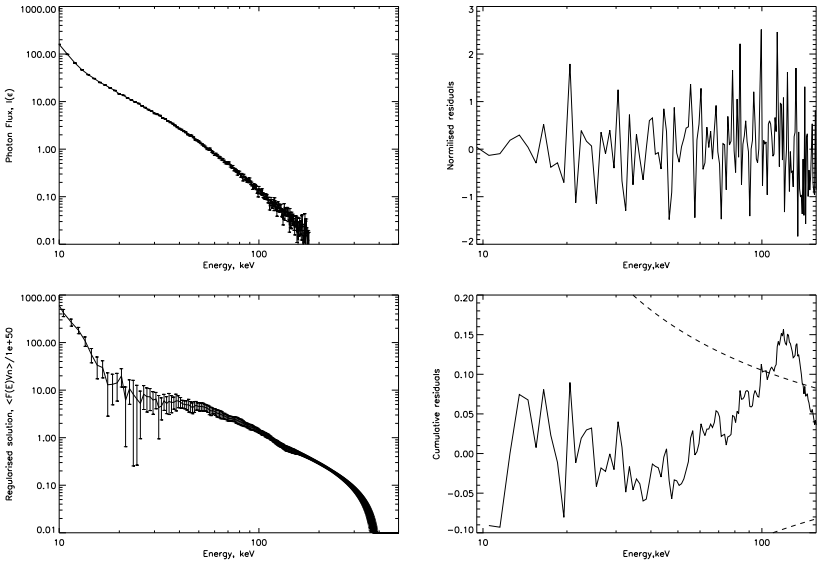

Figure 2. Upper left panel: Photon spectrum for the time interval from 10:26:20-10:26:40 UT, together with spectrum reconstructed from the zero order regularized means source electron spectrum $\overline{F}^{(0)}(E)$, the confidence strip for which is shown in the *lower left panel. Upper right panel:* Normalized residuals between the forward-fit photon spectrum. *Lower right panel:* Corresponding cumulative residuals, compared to the 1σ expectation values for a χ^2 less than 1.

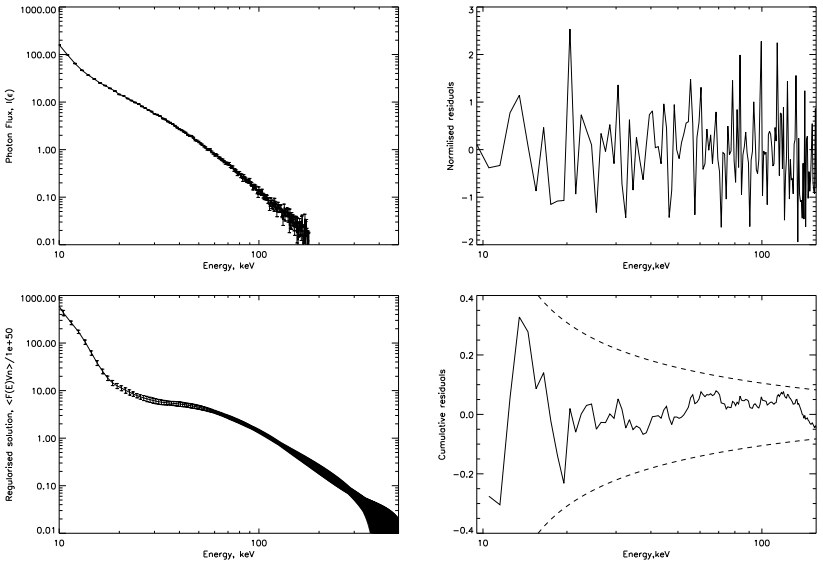

Figure 3. As for Figure 2, for first order regularization.

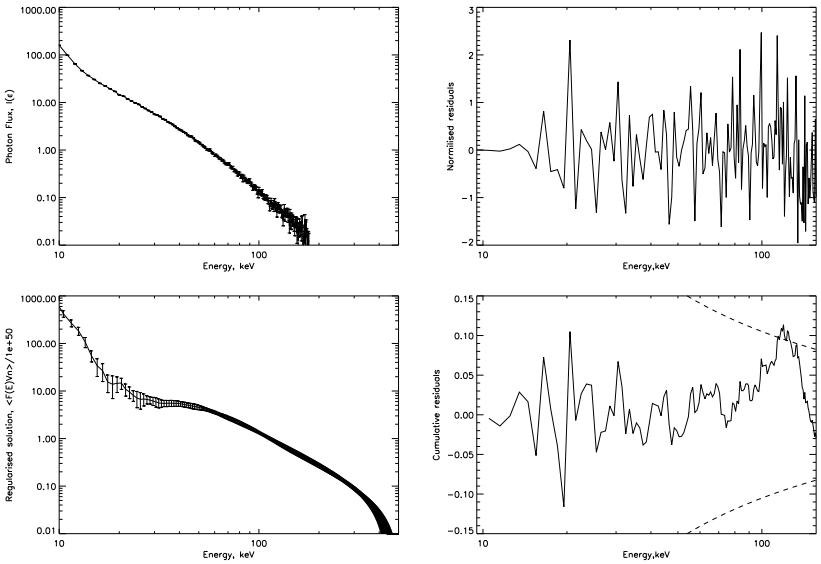

Figure 4. As for Figure 2, for second order regularization.

itself and thus has been ignored (maximum energy in photon spectrum changes from spectrum to spectrum). The photon data used extended over the range $10 \leq \epsilon \leq 160$ keV, while the electron energy band used in the non-square inversion algorithm extended from $10 < E < 480$ keV

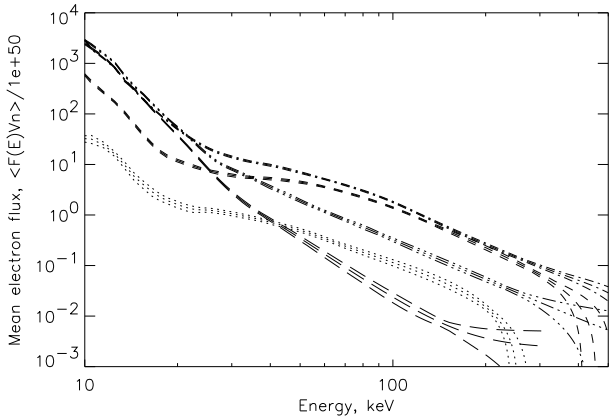

Figure 5. Mean source electron spectra for each time interval of Figure 1; Interval 1-dot line, 2 - dash, 3 - dash dot, 4 - dash three dots, 5 - long dash. Thin lines show 1σ confidence intervals.

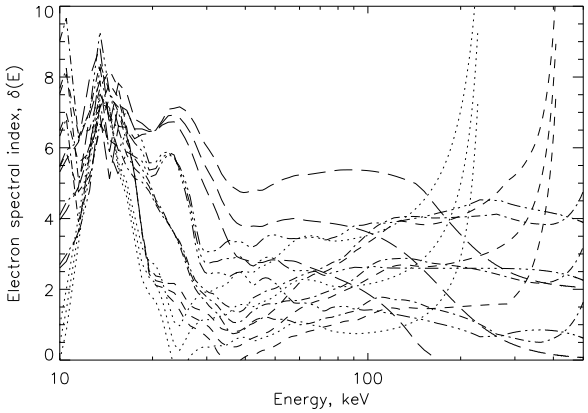

Figure 6. Energy variation of the local spectral index $\delta_E = -d\ln\overline{F}/d\ln E$, obtained using first order regularization techniques for five time intervals (see Figure 5). Thin lines show 1σ error bars.

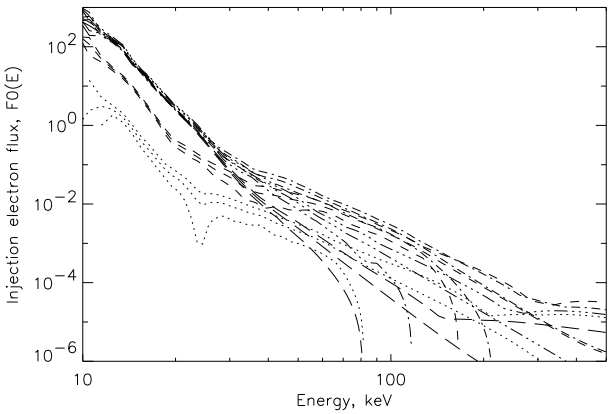

Figure 7. Injected electron spectra $F_0(E_0)$ (arbitrary units) for all 5 time intervals, deduced from the first-order and equation (2). Thin lines show 1σ error bars.

(above 480 keV the solution becomes uncertain). The results are shown as a confidence interval, i.e. a series of realizations of $\overline{F}(E)$, each corresponding to a different noise realization of the photon spectrum, with the noise level determined by the uncertainty in each photon energy bin.

The photon spectrum reconstructed from the mean of this confidence strip is shown overlaid on the data in the top left panel of Figure 2, while the top right panel of that Figure shows the residuals (data –

reconstructed spectrum), normalized to the standard deviation at each energy. The lower right panel of Figure 2 shows that the cumulative residuals (Paper I) mostly fall within the bound, indicating that the recovered mean source electron spectrum $\overline{F}(E)$ reproduces the observed photon spectrum well, with no systematic differences between the forward-fitted spectrum and the original data.

Figure 3 shows the same quantities as Figure 2, for the same photon spectrum, but now using a *first*-order regularization algorithm (see Appendix A of Paper I). Since first-order regularization techniques seek to minimize the norm of the *derivatives* (rather than the amplitude) of $\overline{F}(E)$, the form of $\overline{F}(E)$ is "smoother" than that of $\overline{F}(E)$, particularly where the slope of $\overline{F}(E)$ changes somewhat abruptly (e.g., at the transition from "thermal" to "non-thermal" form at around 30 keV). The residuals are similarly well-behaved to those for the zero order regularization (Figure 2).

Figure 4 shows the same quantities, but the spectrum is smoother in some ranges and is not for other regions. The lack of smoothness in the solution indicates difficulties to approximate an electron spectrum with differentiable functions in that region of energies.

Note, that the error bars (Paper I) in all the figures are at 1σ level (65% confidence). Therefore, the errors do not allow us conclude that the feature near 20 keV seen in Figure 2 and Figure 4 is real.

3. Mean Electron Spectrum

The mean electron spectrum using zero order regularization $\overline{F}(E)$ for the time interval (10:26:20-10:26:40 UT) is shown in the Figure (2).

It should be noted that the high-energy cutoffs revealed by this analysis are all at an energy well above the maximum photon energy sampled. Inversions of the same data set using a binned matrix method (Johns & Lin 1992) yield similar results (with much coarser energy resolution) for the mean source electron spectrum below 200 keV (Johns-Krull, personal communication) but, by the intrinsic nature of the matrix inversion method, it cannot provide unbiased information on the electron spectrum above $E = \epsilon_{\max}$.

We note that both zero order and first order $\overline{F}(E)$ curves become much smoother above $\epsilon_{\max}$, because of the lack of (noisy) data at such high energies. This result illustrates convincingly the power of the regularization technique to use subtle features in the photon spectrum to provide valuable information on the source electron spectrum over a wide range of energies (Paper I).

4. Injected Electron Spectra

The spectra $\overline{F}(E)$ defined by Equation (1) are *mean source electron spectra*, and so represent (density-weighted) averages of the electron flux spectra over the entire source (Brown, Emslie, & Kontar 2003). Emslie (2003) has provided a formula (his Equation [5]) linking the *injected* electron spectrum $F_0(E_0)$ to $\overline{F}(E)$, for a given energy loss model for the electrons. If we approximate the target by a fully ionized "cold" target, then we recover Emslie's Equation (6), viz. (see Brown & Emslie 1988)

$$F_0(E_0) = \frac{\overline{n}V}{A}\, K\, \frac{\overline{F}(E_0)}{E_0^2} \left(1 - \frac{d\ln \overline{F}}{d\ln E}\right)_{E=E_0} . \qquad (2)$$

The appearance of the derivative $d\ln\overline{F}/d\ln E$ in this expression means that in calculating injected electron spectra $F_0(E_0)$, it is important to accurately estimate not only $\overline{F}(E)$, but also its logarithmic slope. Hence regularized solutions that seek to minimize variations in this slope from point to point will produce smoother forms of $F_0(E_0)$.

Figure 6 shows the variation of the local spectral index $\delta_E = -d\ln\overline{F}/d\ln E$ with E. Because the second-order regularization method is specifically designed to minimize fluctuations in the second derivative, the variation of the first derivative (and so δ_E) is much smoother than for the other two orders of regularization. We therefore expect that a second-order regularization method will produce the smoothest forms of the injected electron spectrum $F_0(E_0)$.

Figure 7 shows the forms of the injected spectrum $F_0(E_0)$ in arbitrary units for all five time interval using first order regularization methods. As expected, the second order solution $F_0(E_0)$ shows the most "reasonable" behavior. Not surprisingly, the injected electron spectra show high-energy cutoffs at values similar to that of the corresponding mean source electron spectra.

5. Summary and Discussion

The most important result of this study is that hard X-ray spectra over a finite range of photon energies still carry vital information on the responsible electron spectrum at electron energies substantially higher than the maximum photon energy observed, and that this information can be extracted quantitatively using a non-square Tikhonov regularization technique (Paper I). Further, use of higher-order regularization techniques can produce mean source electron spectra with forms

suitable for further analysis, such as the calculation of the electron spectrum, injected into a collisional thick target, that produces the inferred mean source electron spectrum.

Application of this technique to a flare on February 26, 2002 has shown that the maximum accelerated electron energy rises and falls with time after the peak of the event, concurrent with a growing low-energy thermal component of the hard X-ray emission.

This reduction in the maximum accelerated electron energy may be associated with the changing atmospheric conditions evidenced by the enhanced thermal emission at these later times; the increase in soft X-ray emission may be connected with a larger coronal density which may act to suppress electron acceleration to high energies. Electrons subjected to an applied electric field $\mathcal{E}$ obey the equation of motion

$$\frac{dE}{ds} = e\,\mathcal{E}\left\{1 - \left(\frac{v_t}{v}\right)^2 \frac{\mathcal{E}_D}{\mathcal{E}}\right\}, \tag{3}$$

where e is the magnitude of the electronic charge, v_t is the electron thermal velocity and $\mathcal{E}_D \simeq 10^{-7} n/T$ (V cm^{-1}) is the Dreicer field (Dreicer, 1959). They therefore suffer runaway accleration above a critical velocity

$$v_{\rm crit} = v_t \sqrt{\mathcal{E}_D/\mathcal{E}}. \tag{4}$$

The electrons that suffer runaway acceleration emerge from an acceleration region of length L with an energy given by the solution of Equation (3). As the density n increases, commensurate with the increased emission measure evidenced by the enhanced thermal emission at later time intervals (Figure 5), the value of the Dreicer field is correspondingly increased, the ratio $\mathcal{E}_D/\mathcal{E}$ increases and, by Equation (3), the net force on each electron, and hence its emergent energy ("injection energy") is decreased.

Acknowledgment

This work was supported by NASA's Office of Space Science through Grants NAG5-207745, by a PPARC rolling grant, and by a collaboration grant from the Royal Society.

References

Brown, J.C., & Emslie, A.G.: 1988, *Astrophys. J.*, **331**, 554
Brown, J.C., Emslie, A.G., & Kontar, E.P.: 2003, *Astrophys. J. Lett.*, **595**, L115
Dreicer, H.: 1959, *Physical Review*, **115**, 238

Emslie, A.G.: 2003, *Astrophys. J. Lett.*, **595**, L119
Emslie, A.G., Kontar, E. P., Krucker, S., and Lin, R.P.: 2003, *Astrophys. J. Lett.*, **595**, L117.
Haug, E.: 1997, *Astron. Astrophys.*, **326**, 417
Holman, G. D., Sui, L., Schwartz, R. A., & Emslie, A. G.: 2003, *Astrophys. J. Lett.*, **595**, L97
Johns, C., & Lin, R. P.: 1992, *Solar Phys.*, **137**, 121
Lin R.P., et al.: 2002, *Solar Phys.*, **210**, 3
Lin R.P., et al.: 2003, *Astrophys. J.*, **595**, L69
Kontar, E.P., Brown, J.C., Emslie, A.G., Schwartz, R.A., Smith, D.M., and Alexander, R.C.: 2003, *Astrophys. J. Lett.*, **595**, L123.
Kontar, E. P., Piana, M., Massone, A.M., Emslie, A.G., & Brown, J.C.: 2004, *Solar Phys.*, this volume (Paper I).
Piana, M., Massone, A. M., Kontar, E.P., Emslie, A.G., Brown, J.C., & Schwartz, R.A. 2003, *Astrophys. J. Lett.*, **595**, L127
Smith, D.M. et al.: 2002, *Solar Phys.*, **210**, 33